

# Topological charge Fano effect in multi-Weyl semimetals

W.C. Silva,<sup>1</sup> W.N. Mizobata,<sup>1</sup> J.E. Sanches,<sup>1</sup> L.S. Ricco,<sup>2</sup> I.A. Shelykh,<sup>2,3</sup>  
M. de Souza,<sup>4</sup> M.S. Figueira,<sup>5</sup> E. Vernek,<sup>6</sup> and A.C. Seridonio<sup>1,\*</sup>

<sup>1</sup>São Paulo State University (Unesp), School of Engineering,

Department of Physics and Chemistry, 15385-000, Ilha Solteira-SP, Brazil

<sup>2</sup>Science Institute, University of Iceland, Dunhagi-3, IS-107, Reykjavik, Iceland

<sup>3</sup>ITMO University, St. Petersburg, 197101, Russia

<sup>4</sup>São Paulo State University (Unesp), IGCE, Department of Physics, 13506-970, Rio Claro-SP, Brazil

<sup>5</sup>Instituto de Física, Universidade Federal Fluminense, 24210-340, Niterói, Rio de Janeiro, Brazil

<sup>6</sup>Instituto de Física, Universidade Federal de Uberlândia, Uberlândia, 38400-902, Minas Gerais, Brazil

We theoretically analyze the Fano interference in a single impurity multi-Weyl semimetal hybrid system and show the emergence of the topological charge Fano effect in the bulk local density of states. In multi-Weyl semimetals, the number of Fermi arcs at the system boundaries is determined by the topological charge  $J$ , a direct consequence of the “bulk-boundary” correspondence principle. Analogously, we find that  $J$  also modulates the bulk Fano profile of the system with an embedded quantum impurity. Thus, by increasing  $J$ , the Fano lineshape evolves from resonant, typical for  $J = 1$  (single Weyl), towards antiresonant, extrapolating to the so-called hyper Weyl semimetals with  $J \gg 1$ . Specially for the maximum case protected by the rotational symmetry  $C_{2J=6}$ , namely the  $J = 3$  (triple Weyl), which acquires asymmetric Fano profile, the Fano parameter absolute value is predicted to be  $\tan(C_{2J=6})$ , where  $C_{2J} \equiv (360^\circ/2J)$  defines the rotational angle. Hence, the Fano discretization in the  $J$  term introduces the topological charge Fano effect in multi-Weyl semimetals.

*Introduction.*— Multi-Weyl semimetals[1–8] are intriguing generalizations of standard Weyl semimetals[9–19], once they can lead to a plethora of fascinating effects, such as chiral, optical and transport anomalous properties[7–9, 11, 16–18, 20]. In multi-Weyl semimetals, the band-structures at the so-called Weyl crossing points, show highly anisotropic dispersion relations, being relativistic exclusively in one momentum direction, while in the other two, a power-law dependence is ruled by the topological charge  $J$ [19]. This topological number corresponds to the quantized Berry phase of the Dirac fermions in graphene[21]. As Weyl points appear in pairs with opposite chiralities, they behave as source and drain of an Abelian Berry curvature, thus mimicking (anti)monopoles placed far apart in the reciprocal space. Amazingly, such points are connected to each other via crystal boundaries, in particular, by opened surface states known as Fermi arcs. Notably, these exotic states can be observed by ARPES[1, 2] and turn into the experimental proof of the magnetic monopoles existence in the momenta space.

In multi-Weyl semimetals, the winding number also plays the role of a higher topological charge  $J > 1$ [1]. This charge arises from the merging of  $J$  single chiral degenerated Weyl nodes into multi-Weyl points, which are point group symmetry protected up to  $J = 3$ [15], namely, by means of the rotational symmetry  $C_{2J}$ . In this manner, the “bulk-boundary” correspondence dictates that for a given  $J$  value determined in an infinite bulk system,  $J$  pairs of Fermi arcs appear in the corresponding finite version of the setup[10]. Some examples of multi-Weyl materials are  $\text{HgCr}_2\text{Se}_4$  and  $\text{SrSi}_2$  with  $J = 2$  (double

Weyl)[12, 15, 20, 22], and  $\text{A}(\text{MoX})_3$  ( $\text{A}=\text{Rb}$  or  $\text{Tl}$  and  $\text{X}=\text{Te}$ ) with  $J = 3$  (triple Weyl)[13].

In this work, we focus on the “bulk-boundary” correspondence for Fermi arcs surface states and the topological charge from the bulk, in order to present the concept of the topological charge Fano effect in multi-Weyl semimetals. To this end, we theoretically explore the bulk Fano interference[23, 24] in the LDOS (*local density of states*) for a single impurity multi-Weyl semimetal hybrid system, as sketched in Fig.1(a). As a matter of fact, the Fano interference arises from the coupling between a discrete energy level and an energy continuum[24]. It has been widely investigated in several platforms, ranging from classical mechanics[25] to topological superconductivity[26, 27]. Coupled harmonic oscillators with a driving force[25], photonic systems[28], Jaynes-Cummings-like cavities[29], electronic quantum transport setups made of Anderson adatoms[30–33], atomically frustrated molecules in Weyl metals[8] and topological superconducting nanowires with quantum dots[27], among others[24], constitute the broad variety of examples where Fano interference manifests itself.

Here, we reveal that the increase of  $J$  modifies the bulk Fano profile of a multi-Weyl semimetal with a single impurity, by means of the tuning of Fano asymmetry parameter  $q_J$ , from resonant lineshape ( $|q_{J=1}| \rightarrow \infty$ ) towards antiresonant one ( $|q_{J \gg 1}| \rightarrow 0$ ). We highlight that while the former identifies  $J = 1$  case (single Weyl) [inset panel of Fig.1(b)], the latter predicts a Fano antiresonant profile characterized by  $J \gg 1$ . For such a case, we relax, as we shall clarify later on, the aforementioned crystalline protection[15] and make explicit that the fingerprint for this situation, which we introduce as the hyper Weyl semimetal, is represented by a suppressed Fano parameter ( $|q_{J \gg 1}| \rightarrow 0$ ) [inset panel of Fig.1(d)].

\* corresponding author: [antonio.seridonio@unesp.br](mailto:antonio.seridonio@unesp.br)

We clarify that hyper Weyl semimetals should be understood as a conjecture, being a hypothetical case corresponding to a huge topological charge. However, some research groups have reported spinless platforms with  $J = 4$ [34, 35], pointing out that it is still capital to consider a generalized description. Noteworthy, for  $J \geq 3$ , the Fano parameter becomes finite, discretized in  $J$  and shows a decaying behavior. Particularly for the maximum allowed case by the point symmetry group protection, i.e., the  $J = 3$  value for the  $C_{2J=6}$  rotational symmetry group, we predict  $|q_{J=3}| = \tan(C_{2J=6})$ , with the rotational angle  $C_{2J} \equiv (360^\circ/2J)$  and an asymmetric Fano lineshape [inset panel of Fig.1(c)]. Thereby, our findings introduce the idea of the topological charge Fano effect in multi-Weyl semimetals.

*The Model.*- The Hamiltonian mimicking our system [Fig.1(a)], with  $\hbar = 1$ , reads  $\mathcal{H} = \mathcal{H}_{\text{Weyl}} + \mathcal{H}_{\text{Imp.}} + \mathcal{H}_{\text{Hyb.}}$ , where

$$\mathcal{H}_{\text{Weyl}} = \sum_{\mathbf{k}s} \psi_{\mathbf{k}s}^\dagger s [D(\tilde{k}_-^J \sigma_+ + \tilde{k}_+^J \sigma_-) + v_F(k_z - sQ)\sigma_z] \psi_{\mathbf{k}s} \quad (1)$$

is the part describing multi-Weyl fermions with spinor  $\psi_{\mathbf{k}s}^\dagger = (c_{\mathbf{k}s\uparrow}^\dagger, c_{\mathbf{k}s\downarrow}^\dagger)$ ,  $c_{\mathbf{k}s\sigma}^\dagger$  ( $c_{\mathbf{k}s\sigma}$ ) for creation (annihilation) of an electron carrying winding number  $J$ , momentum  $\mathbf{k}$ , spin  $\sigma = \uparrow, \downarrow$  and chirality  $s = \pm 1$  for the Weyl nodes  $sQ$ , which break time-reversal symmetry. The nonrelativistic part is expressed in terms of  $\tilde{k}_\pm = (k_x \pm ik_y)/k_D$ , being  $k_D = D/v_F$  ( $D$ ) the *Debye-like* momentum (energy) cutoff as in graphene system[36],  $\sigma_\pm = \frac{1}{2}(\sigma_x \pm i\sigma_y)$  and  $\sigma_z$  are the Pauli matrices. We stress that the winding number  $J$ , namely the topological charge, gives the number of Fermi arcs pairs at the system boundaries, as ensured by the ‘‘bulk-boundary’’ correspondence principle[10]. In the last term of Eq.(1), which is of relativistic-type, the slope of the Dirac cones in the  $z$ -direction of the momentum space is the Fermi velocity  $v_F$ .

The band-structure of Eq.(1) can be computed straightforwardly and leads to the following dispersion relation

$$\varepsilon_{\mathbf{k}s}^\pm = \pm v_F \sqrt{k_{zs}^2 + |\tilde{k}_+|^{2J} k_D^2}, \quad (2)$$

wherein  $+(-)$  corresponds to the conduction (valence) band, with  $k_{zs} = k_z - sQ$  and it is depicted in Figs.1(b)-(d). Additionally, it is worth mentioning that for  $J = 1$  (single Weyl) the Weyl semimetal has well-defined Dirac cones in all momentum directions [Fig.1(b)], while for  $J \gg 1$  we have a hypothetical hyper Weyl semimetal case [Fig.1(d)], in which its band-structure shape saturates due to a huge topological charge. Further, a single Anderson-like impurity[30] can be described by the Hamiltonian

$$\mathcal{H}_{\text{Imp.}} = -\frac{U}{2} + \sum_{\sigma} (\varepsilon_{d\sigma} + \frac{U}{2}) n_{d\sigma} + \frac{U}{2} (\sum_{\sigma} n_{d\sigma} - 1)^2, \quad (3)$$

where the impurity electronic energy level is  $\varepsilon_{d\sigma}$ , with number operator  $n_{d\sigma} = (n_{d\sigma})^2 = d_{\sigma}^\dagger d_{\sigma}$ , being  $d_{\sigma}^\dagger$  ( $d_{\sigma}$ )

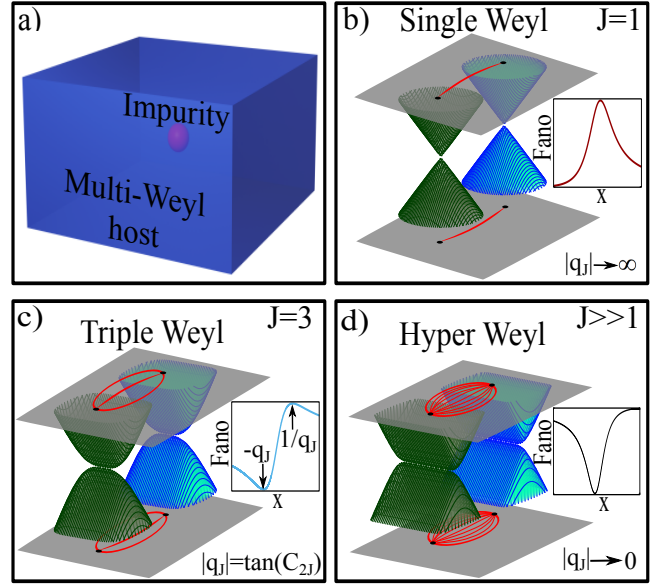


Figure 1. (Color online) Overview of the topological charge Fano effect in multi-Weyl semimetals: (a) Slab of a bulk multi-Weyl semimetal system hosting an impurity. (b)-(d) Qualitative summary of our findings: corresponding band-structures from Eq.(2) with  $k_y = 0$ ,  $Q = 0.4k_D$  and Fermi arcs surface states upon changing the topological charge  $J$ . Related bulk Fano profiles versus the dimensionless resonant energy detuning  $x$  of the impurity appear depicted at the inset panels. The Fano profile evolves from resonant behavior [panel (b)] to the antiresonant-type [panel (d)] as  $J$  increases. The pairs of Fermi arcs are determined by the  $J$  value, which imposes the bulk Fano lineshape. This profile is determined by the absolute value of the Fano asymmetry parameter  $|q_J| = \tan(C_{2J})$  [panel (c)], where  $C_{2J} \equiv (360^\circ/2J)$  stands for the angle of the rotational symmetry group. In summary, the ‘‘bulk-boundary’’ correspondence[10] defines the grounds of the topological charge Fano effect in multi-Weyl systems.

the corresponding creation (annihilation) operator and  $U$  is the Coulomb repulsion between two electrons with opposite spins ( $\bar{\sigma} = -\sigma$ ). The hybridization term, which accounts for the host-impurity coupling, reads

$$\mathcal{H}_{\text{Hyb.}} = v \sum_{\sigma} (f_{0\sigma}^\dagger d_{\sigma} + \text{H.c.}), \quad (4)$$

where the field operator  $f_{0\sigma} = \frac{1}{\sqrt{\mathcal{N}}} \sum_{\mathbf{k}s} c_{\mathbf{k}s\sigma}$  describes the host site locally coupled to an embedded quantum impurity, with  $v$  being the impurity-host coupling strength and  $\mathcal{N}$  the number of states delimited by  $k_D$ .

We would like to call attention to the following: by making the choice  $\varepsilon_{d\sigma} = -\frac{U}{2}$ , the second term of Eq.(3) disappears and the Hamiltonian  $\mathcal{H}$  becomes invariant under the particle-hole transformation  $c_{\mathbf{k}s\sigma} \rightarrow c_{-\mathbf{k}s\sigma}^\dagger$  and  $d_{\sigma} \rightarrow -d_{\sigma}^\dagger$ . This characterizes the particle-hole symmetric regime of the model, which will be employed without loss of generality, in order to determine the system bulk

LDOS. Consequently, the LDOS profile exhibits mirror symmetry in the energy domain  $\varepsilon$  and the bulk Fano profile can be finally known.

*LDOS and Fano profile.*- From the time Fourier transform of the retarded Green's function (GF)  $\mathcal{G}_\sigma = -i\theta(t) \left\langle \left\{ f_{0\sigma}(t), f_{0\sigma}^\dagger(0) \right\} \right\rangle_{\mathcal{H}}$ , i.e.  $\tilde{\mathcal{G}}_\sigma$ , we verify the validity of the Dyson equation  $\tilde{\mathcal{G}}_\sigma = \tilde{\mathcal{G}}_\sigma^0 + \tilde{\mathcal{G}}_\sigma^0 v \tilde{\mathcal{G}}_{\text{Imp.}\sigma} v \tilde{\mathcal{G}}_\sigma^0$  via the equation-of-motion approach[37], with  $\mathcal{G}_\sigma^0$  and  $\mathcal{G}_{\text{Imp.}\sigma} = -i\theta(t) \left\langle \left\{ d_\sigma(t), d_\sigma^\dagger(0) \right\} \right\rangle_{\mathcal{H}}$  representing the pristine multi-Weyl and impurity GFs, respectively. Thus, the Fano formula[23, 24] in the bulk LDOS  $= (-1/\pi)\text{Im}\tilde{\mathcal{G}}_\sigma$  is expected to emerge, if in the impurity DOS  $= (-1/\pi)\text{Im}\tilde{\mathcal{G}}_{\text{Imp.}\sigma}$ , their resonant states[37] exhibit a lorentzian profile.

As we consider the case of  $T \ll T_K \rightarrow 0$  (Kondo temperature)[38] and the system has a pseudogap at the Fermi level, Kondo correlations do not emerge[14] and consequently, the Coulomb blockade regime[37] takes place. The latter is characterized solely by the resonant states  $\varepsilon_{d\sigma}$  and  $\varepsilon_{d\sigma} + U$ , and the correlation  $U$  in  $\tilde{\mathcal{G}}_{\text{Imp.}\sigma}$ , can be safely treated in the framework of the Hubbard-I approximation[7, 8, 37]:

$$\tilde{\mathcal{G}}_{\text{Imp.}\sigma} = -\frac{1}{v^2 \text{Im}\tilde{\mathcal{G}}_\sigma^0} \left( \frac{w_x}{x} + \frac{w_{\bar{x}}}{\bar{x}} \right). \quad (5)$$

This ensures, as expected, the lorentzian lineshape in the DOS.  $\tilde{\mathcal{G}}_\sigma^0 = \frac{1}{N} \sum_{\mathbf{k}s} \frac{\varepsilon + i0^+}{(\varepsilon + i0^+)^2 + (\varepsilon_{\mathbf{k}s}^+)^2}$ , with  $w_x = 1 - \langle n_{d\sigma} \rangle$  and  $w_{\bar{x}} = 1 - w_x$  being spectral weights for the dimensionless resonant energies detuning  $x = \frac{\varepsilon - \varepsilon_{d\sigma} - v^2 \text{Re}\tilde{\mathcal{G}}_\sigma^0}{-v^2 \text{Im}\tilde{\mathcal{G}}_\sigma^0}$  and  $\bar{x} = \frac{\varepsilon - \varepsilon_{d\sigma} - U - v^2 \text{Re}\tilde{\mathcal{G}}_\sigma^0}{-v^2 \text{Im}\tilde{\mathcal{G}}_\sigma^0}$ , respectively, wherein  $\langle n_{d\sigma} \rangle = \int_{-D}^0 \text{DOS} d\varepsilon$  is the impurity occupation.

Now we are able to express the LDOS according to Fano formula[23, 24]. We begin by introducing into  $(-1/\pi)\text{Im}\tilde{\mathcal{G}}_\sigma$ , the quantities as follows:  $\text{Re}\tilde{\mathcal{G}}_\sigma^0 = -\frac{1}{\pi} \int_{-D}^{+D} \frac{\text{Im}\tilde{\mathcal{G}}_\sigma^0}{\varepsilon - y} dy = -\frac{1}{\pi} \text{sgn}(\varepsilon) \text{Im}\tilde{\mathcal{G}}_\sigma^0 \int_{-D/\varepsilon}^{+D/\varepsilon} \frac{(u^2)^{1/J}}{1-u} du = -q_J \text{Im}\tilde{\mathcal{G}}_\sigma^0$ , due to the Kramers-Kronig relations[37], wherein  $y = u\varepsilon$  and the Fano asymmetry parameter is given by

$$q_J = \frac{1}{\pi} \text{sgn}(\varepsilon) \text{P.V.} \int_{-D/\varepsilon}^{+D/\varepsilon} \frac{(u^2)^{1/J}}{1-u} du, \quad (6)$$

where P.V. stands for the Cauchy principal value and

$$\text{Im}\tilde{\mathcal{G}}_\sigma^0 = -\frac{3\pi^{3/2}\Gamma(\frac{1}{J})}{2JD^{\frac{J+2}{J}}\Gamma(\frac{2+J}{2J})} (\varepsilon^2)^{1/J}, \quad (7)$$

with  $\Gamma(x)$  being the Gamma function and the power-law  $(\varepsilon^2)^{1/J}$  is characterized by a pseudogap at the Fermi level ( $\varepsilon = 0$ ).

We emphasize that Eq.(7) holds for arbitrary  $J$  and mention that so far, solely analytical expressions up to  $J = 3$  were obtained[19]. We are aware that the crystalline rotational symmetry  $C_{2J}$  imposes the limitation

$J \leq 3$ , in particular when the spin degree of freedom comes into play[15]. However, the  $J = 4$  case is still possible and emerges in spinless systems[34, 35]. Thus, we develop an extrapolation given by Eq.(7) and get a generalized Fano asymmetry parameter.

The aforementioned accomplishment was possible after employing in  $\tilde{\mathcal{G}}_\sigma^0$  the procedures as follows: (i) the standard substitution  $\mathcal{N} = \sum_{\mathbf{k}s} \rightarrow \frac{\Omega}{(2\pi)^3} \int d^3\mathbf{k} = \frac{\Omega}{6\pi^2} k_D^3$ , with  $\Omega$  as the volume element in real space; (ii) the hyper-spherical transformation given by  $k_x = k_D (\frac{\varepsilon_{\mathbf{k}s}^+ \sin\theta}{D})^{\frac{1}{J}} \cos\phi$ ,  $k_y = k_D (\frac{\varepsilon_{\mathbf{k}s}^+ \sin\theta}{D})^{\frac{1}{J}} \sin\phi$  and  $k_{zs} = k_D \frac{\varepsilon_{\mathbf{k}s}^+}{D} \cos\theta$  ( $0 \leq \theta \leq \pi$ ,  $0 \leq \phi \leq 2\pi$ ), with Jacobian  $J(\varepsilon_{\mathbf{k}s}^+, \theta, \phi) = \frac{k_D^3}{D} (\frac{\varepsilon_{\mathbf{k}s}^+}{D})^{2/J} \frac{(\sin\theta)^{\frac{2}{J}-1}}{J}$  and property  $\int \tilde{\mathcal{G}}_\sigma^0 d^3\mathbf{k} = \int \tilde{\mathcal{G}}_\sigma^0 J(\varepsilon_{\mathbf{k}s}^+, \theta, \phi) d\varepsilon_{\mathbf{k}s}^+ d\theta d\phi$ .

We can finally obtain the bulk Fano profile, which from here, we call by natural Fano profile (NFP), once it is expressed in terms of their natural coordinates  $x$  and  $\bar{x}$ . Taking into account the spin degree of freedom, we find the NFP=2LDOS/ $\rho_0(1+q_J^2)$ , with  $\rho_0 = (-1/\pi)\text{Im}\tilde{\mathcal{G}}_\sigma^0$  as the pristine multi-Weyl DOS and

$$\text{NFP} = \frac{2}{1+q_J^2} \left[ w_x \frac{(x+q_J)^2}{x^2+1} + w_{\bar{x}} \frac{(\bar{x}+q_J)^2}{\bar{x}^2+1} \right], \quad (8)$$

which holds in the wide-band limit  $D/\varepsilon \rightarrow \infty$ . As we are interested in impurity levels nearby the Fermi energy, such a limit prevents that the time-reversal symmetry breaking lifts the system spin degeneracy[14]. From Eq. (8) and for  $\varepsilon < 0$  ( $\varepsilon > 0$ ), the NFP shows amplitudes of minimum and maximum at  $x = -q_J$  ( $\bar{x} = -q_J$ ) and  $x = 1/q_J$  ( $\bar{x} = 1/q_J$ ), respectively.

We highlight that the LDOS spectral lineshape itself, as we shall see in the numerical analysis, will not exhibit a Fano profile as a function of energy  $\varepsilon$  for a given  $q_J$ , as it occurs for flat band systems with energy and  $J$  independent host DOS[31–33]. Additionally, we will verify that for the revealing of such a behavior, one should analyze the Fano profile as a function of  $x$  or  $\bar{x}$ , namely, the natural coordinates for the Fano profile to emerge. Nevertheless, before that, we should firstly evaluate carefully the integral over  $u$  variable in Eq.(6).

We call attention that, in particular for  $q_{J=1}$  and  $q_{J=2}$ , the functions depending on  $u$  do not vanish in the limits  $u \rightarrow \pm\infty$ , which is a common pathology in low-energy models[36]. This feature constitutes a technical difficulty in solving Eq.(6) numerically. Hence, to handle accordingly with this lack of integrability issue, we should, as already performed in graphene system[36], solve first the integral analytically by keeping the ratio  $D/\varepsilon$  finite and assuming later on, the limit  $\varepsilon/D \ll 1$  in the  $\text{Re}\tilde{\mathcal{G}}_\sigma^0$  evaluations. Such cases are then described by

$$\text{Re}\tilde{\mathcal{G}}_\sigma^0(J=1) = \frac{3\varepsilon}{D^3} (\varepsilon \ln \left| \frac{D+\varepsilon}{D-\varepsilon} \right| - 2D) \quad (9)$$

and

$$\text{Re}\tilde{\mathcal{G}}_\sigma^0(J=2) = \frac{3\pi}{4D^2} \varepsilon \ln \left| \frac{\varepsilon^2}{\varepsilon^2 - D^2} \right|, \quad (10)$$

respectively, which provide

$$q_{J \leq 2} = -\frac{\text{Re}\tilde{\mathcal{G}}_\sigma^0(J \leq 2)}{\text{Im}\tilde{\mathcal{G}}_\sigma^0(J \leq 2)} \quad (11)$$

as dependent both on energy for  $\varepsilon/D \ll 1$  and topological charge  $J$ .

However, the necessary vanishing behavior is present in  $q_{J \geq 3}$  as a function of  $u$  and consequently, it makes the integral in Eq.(6) to behave finite for  $D/\varepsilon \rightarrow \infty$ , which can be found analytically simultaneously with the ratio  $D/\varepsilon \rightarrow \infty$ . This results into an interesting finding, i.e., an energy-independent Fano asymmetry parameter discretized in the topological charge  $J$ , which reads

$$q_{J \geq 3} = -\text{sgn}(\varepsilon) \tan(C_{2J \geq 6}), \quad (12)$$

where we define  $C_{2J} \equiv (360^\circ/2J)$  as the angle for the corresponding rotational symmetry group. Together with Eqs.(9), (10) and (11), this gives the set of analytical expressions that defines the topological charge Fano effect in multi-Weyl systems. Notice that for  $J = 3$ ,  $q_{J=3} = -\text{sgn}(\varepsilon) \tan(C_{2J=6}) = -\text{sgn}(\varepsilon)\sqrt{3}$ , while for  $J \gg 1$  we have  $|q_{J \gg 1}| \rightarrow 0$ , which corresponds to the maximum allowed point group symmetry protected case, namely, the  $C_{2J=6}$  rotational symmetry group, and the hypothetical hyper Weyl semimetal, respectively.

*Results and discussion.*- As stated previously, we consider the particle-hole symmetric regime. In this case,  $\varepsilon_{d\sigma} = -\frac{U}{2}$  and  $w_x = w_{\bar{x}} = 1/2$  ( $\langle n_{d\bar{\sigma}} \rangle = 1/2$  from self-consistent calculations), with  $U = v = 0.14D$ . Taking into account Eq.(8), in Fig.2, we present the spectral analysis of the bulk LDOS  $= \rho_0 \frac{(1+q_J^2)}{2}$  NFP as a function of  $\varepsilon$  and the first part of the NFP versus  $x$  for several  $J$  values. As the dimensionless resonant energy detuning  $x$  is proportional to the deviation from the resonant state  $\varepsilon_{d\sigma} = -\frac{U}{2}$  within the valence band, its domain holds for  $\varepsilon < 0$ . Thus, the second part of Eq.(8) as a function of  $\bar{x}$  exhibits a reversed profile, once  $\bar{x} = -x$  in the domain  $\varepsilon > 0$  (conduction band), where the resonant state  $\varepsilon_{d\sigma} + U = \frac{U}{2}$  resides and  $\text{Re}\tilde{\mathcal{G}}_\sigma^0(\varepsilon > 0) = -\text{Re}\tilde{\mathcal{G}}_\sigma^0(\varepsilon < 0)$  fulfills particle-hole symmetry[14]. Hence, the dependence of Eq.(8) on  $\bar{x}$  is not shown, for a sake of simplicity.

Counterintuitively, the LDOS in Fig.2(a) does not show Fano profiles around the resonant states as a function of  $\varepsilon$  upon changing  $J$ , as it should occur, despite the Fano parameters being dictated by Eqs.(11) and (12). Such a feature arises from the topological charge  $J$  and energy  $\varepsilon$  dependencies present in the resonant states broadening  $\Delta = -2v^2 \text{Im}\tilde{\mathcal{G}}_\sigma^0 = 2\pi v^2 \rho_0$  and quasi-particle dressing term  $v^2 \text{Re}\tilde{\mathcal{G}}_\sigma^0$  of the impurity. These quantities, in particular, appear in the resonant energies detuning  $x = 2(\varepsilon - \varepsilon_{d\sigma} - v^2 \text{Re}\tilde{\mathcal{G}}_\sigma^0)/\Delta$  and  $\bar{x} = 2(\varepsilon - \varepsilon_{d\sigma} - U - v^2 \text{Re}\tilde{\mathcal{G}}_\sigma^0)/\Delta$  entering into Eq.(8). From the latter, we perceive that  $x$  and  $\bar{x}$  are not linearly proportional to  $\varepsilon$ . This characteristic is restored when  $\Delta$  and  $v^2 \text{Re}\tilde{\mathcal{G}}_\sigma^0$  become energy and  $J$  independent, as verified

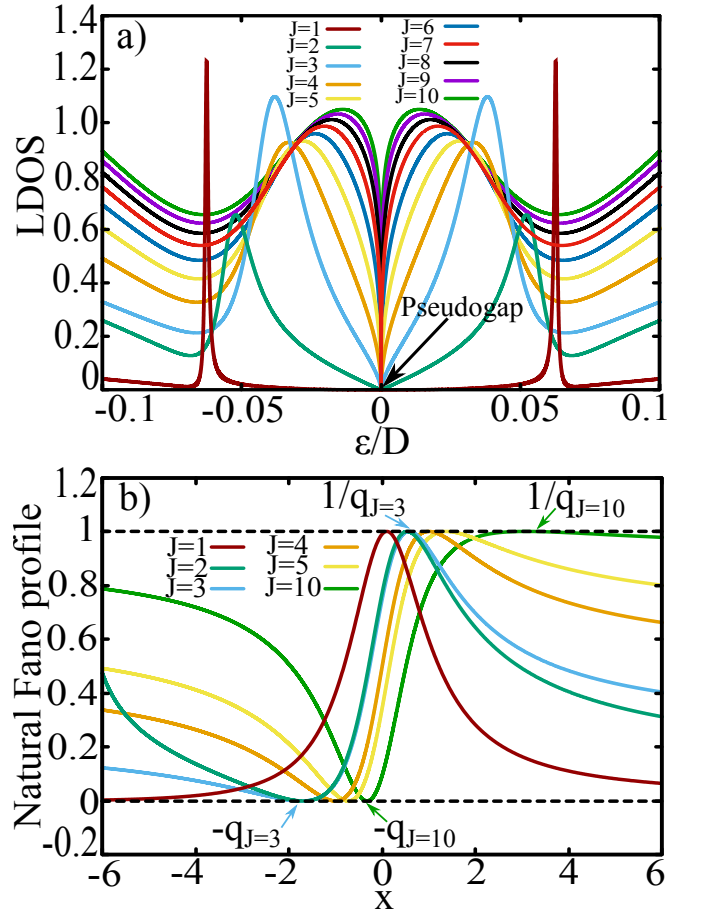


Figure 2. (Color online) (a) LDOS  $= \rho_0 \frac{(1+q_J^2)}{2}$  NFP [Eq.(8)] versus energy  $\varepsilon$  in units of the cutoff  $D$  for several  $J$  values and particle-hole symmetric regime:  $\varepsilon_{d\sigma} = -\frac{U}{2}$  and  $w_x = w_{\bar{x}} = 1/2$ , with  $U = v = 0.14D$  (see the main text). The increase of  $J$  turns the pseudogap flanked by the impurity resonant states more pronounced with a sharp dip. (b) Natural Fano profile NFP [first part of Eq.(8)] versus  $x$  and dependent on  $J$  for  $\varepsilon < 0$ . In the case of  $\varepsilon > 0$ , the profile is just reversed as a function of  $\bar{x}$  and it is not shown, for a sake of simplicity. We clearly verify that  $J$  modulates the Natural Fano profile.

in metallic flat bands near the Fermi level[31–33]. Consequently, solely in this particular situation, the LDOS profile as a function of  $\varepsilon$  shows Fano lineshapes.

Therefore, in the case of multi-Weyl semimetals, one should analyze  $2\text{LDOS}/\rho_0(1+q_J^2)$ , namely, the NFP given by Eq.(8), as a function of the natural coordinate  $x$  or  $\bar{x}$  instead of  $\varepsilon$ , to indeed perceive the emerging NFP around  $x = 0$  or  $\bar{x} = 0$ . Such analysis appears in Fig.2(b), where we verify that the increase of  $J$  drives the system from the resonant Fano profile for the case of single Weyl semimetal  $J = 1$ , towards the hyper Weyl semimetal with  $J \gg 1$ , which is identified by an antiresonant lineshape. Further, the Fano minimum and maximum amplitudes positions for  $\varepsilon < 0$  given by  $x = -q_J$  and  $x = 1/q_J$ , respectively, then appear in such a figure marked by arrows, just in order to make explicit the discretized Fano



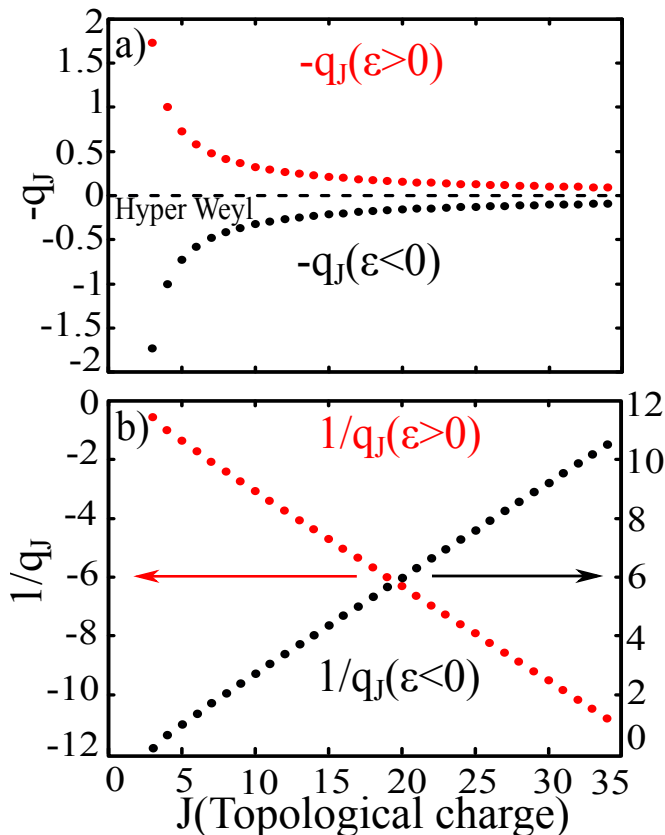


Figure 3. (Color online) (a) Minimum amplitude position  $-q_J$  of the Fano profile from Eq.(12) [see also Figs. 1(c) and 2(b)] with decaying behavior as a function of  $J \geq 3$  for energies  $\varepsilon > 0$  and  $\varepsilon < 0$ . (b) The same for the maximum amplitude position  $1/q_J$ , but with a linear dependence on  $J$ . Panels (a) and (b) make explicit that the Fano asymmetry parameter  $q_J$  given by Eq.(12) consists of a discretized quantity in the  $J$  term, yielding the topological charge Fano effect.

parameter in  $J$ . However, in Fig.2(a) for the LDOS representation as a function of  $\varepsilon$ , the role of  $J$  solely lies in the renormalization of the resonant states towards the Fermi level as  $J$  increases, pointing out that the semimetallic pseudogap becomes characterized by an extremely sharp dip, due to its spectral power-law  $(\varepsilon^2)^{1/J}$  in Eq.(7).

It is worth noting that the discretization observed in Fig.2(b) arises from Eq. (12), which together with Eqs.(9), (10) and (11) are the most capital ones of the current work: they encode the topological charge Fano effect in multi-Weyl systems, once they allow the tuning of the Fano lineshape by changing the topological charge  $J$ . Equivalently, according to the “bulk-boundary” correspondence, the pairs of Fermi arcs surface states present at the system boundaries are fixed by the  $J$  value[10], which also imposes the Fano profile lineshape of the bulk.

With this in mind, we see from Fig.3(a) that for  $\varepsilon < 0$  the limits  $-q_{J \rightarrow 3} \rightarrow -\tan(C_{2J=6}) = -\sqrt{3}$  and  $-q_{J \gg 1} \rightarrow 0$  are reached, while for  $\varepsilon > 0$  we have

$-q_{J \rightarrow 3} \rightarrow \tan(C_{2J=6}) = \sqrt{3}$  and  $-q_{J \gg 1} \rightarrow 0$ . Interestingly enough for  $J = 3$ ,  $|q_{J=3}| = \tan(C_{2J=6}) = \sqrt{3} \approx 1,732$  and the Fano profile, according to Fig.2(b), rises as asymmetric. Particularly for the  $-q_J$  decaying behavior with  $J$  reported in Fig.3(a), we highlight that such a feature is connected straightforwardly to the system band-structure. As stated previously, the band-structure saturates into one characteristic for the hyper Weyl semimetal-type with  $J \gg 1$ , as depicted in Fig.1(d). As an aftermath, if the shape generated by the dispersion  $\varepsilon_{\mathbf{k}s}^{\pm}$  from Eq.(2) remains unchanged by increasing  $J \gg 1$  [Fig.1(d)], so does the Fano parameter, which attains to  $|q_{J \gg 1}| \rightarrow 0$ , once it depends on  $\varepsilon_{\mathbf{k}s}^{\pm}$  via the GF  $\hat{G}_{\sigma}^0$  of the pristine host. As a result, the antiresonant Fano profile becomes the hallmark of hyper Weyl semimetals.

In Fig.3(b), we show the corresponding behavior for  $1/q_J$ , which is linear instead. Note that  $1/q_J$  for  $\varepsilon < 0$  follows an increasing linear trend, while for  $\varepsilon > 0$  it is the opposite. This reflects the own particle-hole symmetry characteristic of the Fano parameter and it occurs because the multi-Weyl points and Fermi level are energy-degenerated. Thereby, the band-structure also has particle-hole symmetry, as well as the  $1/q_J$  quantity. Most importantly, both the  $-q_J$  and  $1/q_J$  behaviors as functions of  $J$  make explicit that the Fano parameter is discretized, thus characterizing the topological charge Fano effect in multi-Weyl semimetals.

*Conclusions.*- In this work, we determine the Fano asymmetry parameter for a single impurity coupled to a multi-Weyl semimetal and introduce the concept of topological charge Fano effect. According to the “bulk-boundary” correspondence, which states that the number of Fermi arcs at the boundaries of a finite size system is determined by the magnitude of the topological charge, known from its bulk version with infinite size, we then reveal the modulation of the system Fano profile, due to the bulk LDOS, by such surface states. This can be emulated in our theoretical framework by the tuning of the topological charge value, which allows the Fano profile to change from resonant pattern for single Weyl semimetal, towards the antiresonant Fano lineshape, which identifies hyper Weyl semimetals. Additionally, for the maximum allowed protected case by the rotational symmetry group  $C_{2J=6}$ , namely, the triple Weyl semimetal  $J = 3$  and rotational angle defined by  $C_{2J} \equiv (360^\circ/2J)$ , we predict the absolute Fano parameter  $|q_{J=3}| = \tan(C_{2J=6})$  and an asymmetric Fano profile.

*Acknowledgments.*- We thank the Brazilian funding agencies CNPq (Grants. Nr. 302887/2020-2, 308410/2018-1, 305738/2018-6, 311366/2021-0 and 305668/2018-8, 308695/2021-6), Coordenação de Aperfeiçoamento de Pessoal de Nível Superior - Brasil (CAPES) – Finance Code 001 and FAPERJ process Nr. 210 355/2018. LSR and IAS acknowledge support from the Icelandic Research Fund (project “Hybrid polaritonics”). IAS also acknowledges support from the Program Priority 2030. LSR thanks ACS and Unesp for their hospitality.

- 
- [1] M. Z. Hasan, G. Chang, I. Belopolski, G. Bian, S.-Y. Xu, and J.-X. Yin, *Nature Reviews Materials* **6**, 784 (2021).
- [2] M. Z. Hasan, S.-Y. Xu, I. Belopolski, and S.-M. Huang, *Annual Review of Condensed Matter Physics* **8**, 289 (2017).
- [3] B. Yan and C. Felser, *Annual Review of Condensed Matter Physics* **8**, 337 (2017).
- [4] H. Zheng and M. Zahid Hasan, *Advances in Physics: X* **3**, 1466661 (2018).
- [5] N. P. Armitage, E. J. Mele, and A. Vishwanath, *Rev. Mod. Phys.* **90**, 015001 (2018).
- [6] J. Hu, S.-Y. Xu, N. Ni, and Z. Mao, *Annual Review of Materials Research* **49**, 207 (2019).
- [7] Y. Marques, W. N. Mizobata, R. S. Oliveira, M. de Souza, M. S. Figueira, I. A. Shelykh, and A. C. Seridonio, *Scientific Reports* **9**, 8452 (2019).
- [8] W. N. Mizobata, Y. Marques, M. Penha, J. E. Sanches, L. S. Ricco, M. de Souza, I. A. Shelykh, and A. C. Seridonio, *Phys. Rev. B* **102**, 075120 (2020).
- [9] S. Park, S. Woo, E. J. Mele, and H. Min, *Phys. Rev. B* **95**, 161113 (2017).
- [10] R. M. A. Dantas, F. Peña-Benitez, B. Roy, and P. Surówka, *Phys. Rev. Research* **2**, 013007 (2020).
- [11] T. Hayata, Y. Kikuchi, and Y. Tanizaki, *Phys. Rev. B* **96**, 085112 (2017).
- [12] G. Xu, H. Weng, Z. Wang, X. Dai, and Z. Fang, *Phys. Rev. Lett.* **107**, 186806 (2011).
- [13] Q. Liu and A. Zunger, *Phys. Rev. X* **7**, 021019 (2017).
- [14] G. T. D. Pedrosa, J. F. Silva, and E. Vernek, *Phys. Rev. B* **103**, 045137 (2021).
- [15] C. Fang, M. J. Gilbert, X. Dai, and B. A. Bernevig, *Phys. Rev. Lett.* **108**, 266802 (2012).
- [16] R. M. A. Dantas, F. Peña-Benitez, B. Roy, and P. Surówka, *Journal of High Energy Physics* **2018**, 69 (2018).
- [17] S. Ahn, E. J. Mele, and H. Min, *Phys. Rev. B* **95**, 161112 (2017).
- [18] S. P. Mukherjee and J. P. Carbotte, *Phys. Rev. B* **97**, 045150 (2018).
- [19] H.-F. Lü, Y.-H. Deng, S.-S. Ke, Y. Guo, and H.-W. Zhang, *Phys. Rev. B* **99**, 115109 (2019).
- [20] Q. Chen and G. A. Fiete, *Phys. Rev. B* **93**, 155125 (2016).
- [21] A. H. Castro Neto, F. Guinea, N. M. R. Peres, K. S. Novoselov, and A. K. Geim, *Rev. Mod. Phys.* **81**, 109 (2009).
- [22] S.-M. Huang, S.-Y. Xu, I. Belopolski, C.-C. Lee, G. Chang, T.-R. Chang, B. Wang, N. Alidoust, G. Bian, M. Neupane, D. Sanchez, H. Zheng, H.-T. Jeng, A. Bansil, T. Neupert, H. Lin, and M. Z. Hasan, *Proceedings of the National Academy of Sciences* **113**, 1180 (2016).
- [23] U. Fano, *Phys. Rev.* **124**, 1866 (1961).
- [24] A. E. Miroshnichenko, S. Flach, and Y. S. Kivshar, *Rev. Mod. Phys.* **82**, 2257 (2010).
- [25] Y. S. Joe, A. M. Satanin, and C. S. Kim, *Physica Scripta* **74**, 259 (2006).
- [26] J. J. Xia, S. Q. Duan, and W. Zhang, *Nanoscale Research Letters* **10**, 223 (2015).
- [27] L. S. Ricco, V. L. Campo, I. A. Shelykh, and A. C. Seridonio, *Phys. Rev. B* **98**, 075142 (2018).
- [28] M. F. Limonov, M. V. Rybin, A. N. Poddubny, and Y. S. Kivshar, *Nature Photonics* **11**, 543 (2017).
- [29] J. Gollwitzer, L. Bocklage, R. Röhlberger, and G. Meier, *npj Quantum Information* **7**, 1 (2021).
- [30] P. W. Anderson, *Phys. Rev.* **124**, 41 (1961).
- [31] V. Madhavan, W. Chen, T. Jamneala, M. Crommie, and N. Wingreen, *Science* **280**, 567 (1998).
- [32] N. Knorr, M. A. Schneider, L. Diekhöner, P. Wahl, and K. Kern, *Phys. Rev. Lett.* **88**, 096804 (2002).
- [33] O. Újsághy, J. Kroha, L. Szunyogh, and A. Zawadowski, *Phys. Rev. Lett.* **85**, 2557 (2000).
- [34] C. Cui, X.-P. Li, D.-S. Ma, Z.-M. Yu, and Y. Yao, *Phys. Rev. B* **104**, 075115 (2021).
- [35] T. Zhang, R. Takahashi, C. Fang, and S. Murakami, *Phys. Rev. B* **102**, 125148 (2020).
- [36] B. Uchoa, V. N. Kotov, N. M. R. Peres, and A. H. Castro Neto, *Phys. Rev. Lett.* **101**, 026805 (2008).
- [37] H. Bruus and K. Flensberg, *Many-Body Quantum Theory in Condensed Matter Physics, An Introduction* (Oxford: Oxford University Press) (2012).
- [38] A. C. Hewson, *The Kondo Problem to Heavy Fermions* (Cambridge: Cambridge University Press) (1993).